
Article:
Ali, H.T., Ramzan, M., Arshad, M.I. et al. (8 more authors) (2022) Tailoring the optical, and magnetic properties of La-BaM hexaferrites by Ni substitution. Chinese Physics B, 31 (2). 027502. ISSN 1674-1056

https://doi.org/10.1088/1674-1056/ac1412

Chinese Physics B

Tailoring the optical, and magnetic properties of La-BaM hexaferrites by Ni substitution

To cite this article before publication: Hafiz T. Ali *et al* 2021 *Chinese Phys. B* in press https://doi.org/10.1088/1674-1056/ac1412

Tailoring the optical, and magnetic properties of La-BaM hexaferrites by Ni substitution

Hafiz T. Ali[1], M. Ramzan[2], M Imran Arshad[2], Nicola A. Morley[3], M. Hassan Abbas[2], Mohammad Yusuf[4], Atta Ur Rehman[2], Khalid Mahmood[2], Adnan Ali[2], Nasir Amin[2], M. Ajaz-un-Nabi[2,*]

[1] Department of Mechanical Engineering, College of Engineering, Taif University, P.O. Box 11099, Taif 21944, Saudi Arabia

[2]Department of Physics, Government College University, Faisalabad, Pakistan

[3] Department of Materials Science and Engineering, University of Sheffield, Sir Robert Hadfield Building, Mapping St., Sheffield, S1 3JD, UK

[4] Department of Clinical Pharmacy, College of Pharmacy, Taif University, P.O. Box 11099, Taif 21944, Saudi Arabia

*majazunnabi@gcuf.edu.pk

Abstract

The impact of Ni insertion on structural, optical, and magnetic properties of $Ba_{0.8}La_{0.2}Fe_{12-x}Ni_xO_{19}$ hexaferrites (Ni substituted La-BaM hexaferrites) is investigated. The samples were prepared using the conventional co-precipitation method and sintered at 1000 ^oC for 4 hours to assist the crystallization process. The analysis of the structure of the samples was carried out using X-ray diffraction (XRD) spectrometer. The M-type hexagonal structure of all the samples was confirmed from the XRD spectra. The lattice parameters 'a' and 'c' are found in the range 5.8925 ± 0.001 - 5.8952 ± 0.001 nm and 23.2123 ± 0.001 - 23.2219 ± 0.001 nm, respectively. The M-type hexagonal nature of the prepared samples is also indicated by the presence of corresponding FT-IR bands and Raman modes in the FT-IR and Raman spectra, respectively. The EDX results confirmed the successful synthesis of the samples according to the required stoichiometric ratio. UV-vis spectrometer was used to record the absorption spectra of the prepared samples in the wavelength range 200 – 1100 nm. The optical energy band gap of the samples were found in the range 1.21 – 3.39 eV. The M-H loops of the samples were measured at room temperature in the applied magnetic field range 0 – 60 KOe. A high saturation magnetization of 99.92 emu/g was recorded in the sample with x = 0 and with microwave operating frequency 22.2 GHz. This high value of saturation magnetization is due to the substitution of La^{3+} ions at spin-up (12k, 2a, and 2b) sites. The Ni substitution is proved to be a potential candidate to tune the optical and magnetic parameters of M-type hexaferrites. Therefore, the prepared samples are suggested for applications in magneto-optic applications.

Keywords: M-type hexaferrite; Nanostructured materials; magnetic properties; optical properties

1. Introduction

In recent years, hexagonal magnetic nanoparticles have attracted great scientific interest due to their potential for various technological applications like permanent magnets, microwave absorbers, high-density magnetic media, magneto-optic recording media, stealth technology [1-4]. Hexagonal ferrites are divided into five sub-categories based on their crystal structure and chemical formula: M-type ($AFe_{12}O_{19}$), W-type ($AFe_{16}O_{27}$), X-type ($AFe_{28}O_{46}$), Y-type ($AFe_{12}O_{22}$), Z-type ($AFe_{24}O_{41}$), where A is the divalent cation like Ba^{2+}, Sr^{2+}, Pb^{2+}, Ca^{2+} [5-7]. Among these, M-type hexaferrite has gained more attention due to its distinguished properties like very high magnetic anisotropy, higher coercivity, higher corrosion resistance, high thermal and chemical stability [8-11]. Barium M-type (BaM) hexaferrite are ferrimagnetic materials with the chemical formula $BaFe_{12}O_{19}$ and space group $P6_3/mmc$. They consist of tetrahedral ($4f_1$), octahedral ($12k$, $4f_2$, and $2a$) and hexahedral ($2b$) sites. Fe^{3+} ions at $4f_1$ and $4f_2$ sites (eight ions per unit cell) exhibit spin-down character and Fe^{3+} ions at $12k$, $2a$, and $2b$ sites (sixteen ions in a unit cell) exhibit spin-up character [12-13]. The substitution of various magnetic and non-magnetic ions at these sites can modify the structural, magnetic, and other properties of BaM ferrites. Various examples of substitution at different sites of hexaferrite structure are divalent ions (A^{2+}) substitution [14, 15], trivalent ions (A^{3+}) substitution [16, 17], and tetravalent ions (A^{4+}) substitution [14, 18]. To achieve the best properties of hexaferrite, it is very important to optimize the quantity and type of the substituent cations. Various reports have been published on modifying the microstructure, electrical, dielectric, optical, and magnetic properties of BaM hexaferrite by replacing Fe^{3+} and Ba^{3+} cations with divalent and trivalent cations. Recently, Cernea et al. [9] reported on the magnetic properties of Ni^{2+} substituted $BaFe_{12}O_{19}$ hexaferrite. They observed a decreasing trend in the coercivity, retentivity, and maximum energy product with an increase in Ni^{2+}. Iqbal *et al*. [19] studied the effect of Pr-Ni substitution in the crystal lattice of BaSr hexaferrite. They reported an increase in the electrical resistivity of prepared samples with an increase in Ni content. Behera *et al*. [20] also investigated the effect of Ni^{2+} incorporation in the lattice matrix of $BaFe_{12}O_{19}$ synthesized by the sol-gel method. They have found the reduction in saturation magnetization from 68.16 emu/g to 58.99 emu/g with increasing Ni^{2+} content (x) from 0 to 0.5, while an increase in ferrimagnetic transition temperature (T_C) was observed. Guner *et al*. [21] reported the synthesis of Bi and La-doped BaM hexaferrite by sol-gel auto combustion method. They studied the dependence of the magnetic properties of $BaFe_{12}O_{19}$ on the concentration of various dopants like La, Bi, and Y. They reported the saturation magnetization and coercivity of the prepared samples in the range 53.69 – 67.42

emu/g and $3.812 \times 10^5 - 2.177 \times 10^5$ A/m, respectively. Some other attempts also have been reported to modify the structure, electrical, optical, and magnetic properties of BaM with doping of Ni^{2+}, La^{3+}, and co-doping of these cations [19, 22-25]. However, a detailed study is still needed to explore the impact of Ni^{2+} doping on the structural, optical, and magnetic properties of La-BaM hexaferrites. The high coercivity, moderate saturation magnetization, and low cost are all advantages of these materials. The objective of this work is to provide a detailed study on the impact of Ni^{2+} substitution in La-BaM hexaferrites. A series of samples having the chemical formula $Ba_{0.8}La_{0.2}Fe_{12-x}Ni_xO_{19}$ (Ni-doped BL) hexaferrites has been prepared *via* the co-precipitation route. The co-precipitation method was chosen due to its simplicity, low cost, normal temperature, less time required, and homogeneity of prepared nanoparticles [26, 27]. The prepared samples were investigated using different techniques including X-ray diffraction (XRD), Energy Dispersive X-rays (EDX) spectroscopy, Fourier Transform Infrared (FTIR) spectroscopy, Raman Spectroscopy, UV-vis spectroscopy, and Vibrating Sample Magnetometry (VSM).

2. Experimental details

2.1 Synthesis

In this study, $Ba_{0.8}La_{0.2}Fe_{12-x}Ni_xO_{19}$ (x = 0, 0.1, 0.2, 0.3, 0.4, 0.5) ferrites were prepared by the co-precipitation method. The starting materials $BaCl_2.2H_2O$, Ni $(NO_3)_2.6H_2O$, Fe $(NO_3)_3.9H_2O$, and La $(NO_3)_3.6H_2O$ were purchased from Aldrich and used as received. The required amount of these chemicals was used to prepare a homogeneous solution into deionized water according to the required stoichiometric ratios. The solution was stirred magnetically at the hotplate at temperature 70 ^oC till the formation of precipitates occurred. The pH of the solution was maintained during the precipitation process at 11 by adding NaOH dropwise. The samples were placed in the water bath for 12 hours at 90 ^oC to complete the digestion process. The precipitates were laid down at the bottom of the beakers. These precipitates were collected and cleaned with DI water and ethanol to get rid of the impurities. The drying of washed precipitates was done by placing them in the oven for 15 hours at 110 ^oC. The dried precipitates were ground using mortar and pestle to obtain fine powder samples. The samples were sintered at 1000 ^oC in the muffle furnace for 4 hours to assist the crystallization process. The cooling was done at a very slow rate ($\approx$ 1.4 ^oC) to avoid the development of pores.

2.2 Characterization used

The phase and microstructure analysis of the sintered samples was carried out using X-ray diffractometer (D8 Advance, Bruker), with $Cu_{k\alpha}$ as X-ray source. The diffraction patterns were recorded in the 2θ range of 20-60 degrees. The FT-IR spectrometer (spectrum 2, Perkin Elmer) was used to obtain the infrared spectra. An Energy Dispersive X-ray spectrometer was used to determine the elemental composition of prepared samples. Raman spectra were recorded in the wavenumber range 150 – 800 cm^{-1} using a Raman spectrometer. The optical energy band gap values were determined using a UV-Vis spectrometer (double beam, Lambda 25, Perkin Elmer). The magnetic character of the sintered samples was studied by recording *M-H* loops at room temperature using a vibrating sample magnetometer (Lakeshore-7407).

3. Results and Discussion

3.1 Phase analysis

XRD spectra of synthesized Ni-doped La-BaM hexaferrites as shown in Fig. 1 were recorded at 300 K. The comparison of XRD patterns revealed that all the labeled peaks are well-matched with JCPDS data (card #00-051-1879) BaM hexaferrites and no extra peak was observed. It confirms the formation of a single-phase magneto-plumbite structure having space group $P6_3/mmc$ with very high accuracy and without any defect or impurity phase. The various crystal structure parameters including lattice constants (*a* & *c*) [28], crystallite size, unit cell volume [8], X-ray density [26], and dislocation density [29, 30] are calculated utilizing the indexed XRD patterns and the calculated parameters are presented in Table 1. From Fig. 2, it can be observed that the lattice constants "*a*" increased with increased Ni^{2+} ions content, and "*c*" also increased with the addition of doping except $x = 0.3$. It also found from Figure 2 that the unit cell volume (*V*) enhanced with the substitution of dopant ions. This increase is attributed to the difference in ionic radii of Ni^{2+} (0.69 Å) and Fe^{3+} (0.64 Å) [20]. The average crystallite size of the prepared nanoparticles was found in the range 25.2 ± 0.1 – 28.5 ± 0.1 nm and showed a decreasing trend with an increase in Ni^{2+} ions concentration. The calculated X-ray density of the samples was found to lie in the range 5.144 – 5.310 g/cm^3. The dislocation density of a material is inversely proportional to the square of the crystallite size and provides information about the strength of the materials [29, 30]. The calculated values of dislocation density of the prepared nanoparticles revealed that the sample with $x = 0.1$ has the minimum value of dislocation density.

3.2 Elemental Composition analysis

The elemental composition of the synthesized samples were analyzed quantitatively using Energy dispersive X-rays (EDX) spectroscopy and the results are presented in Table 2.

The observed composition of all the elements well matched the expected stoichiometric composition. The results confirmed that La^{3+} and Ni^{2+} cations substituted in Ba and Fe cations in the appropriate ratios.

3.3 Functional group analysis

The FTIR spectra of the prepared powder were recorded in the range 4000 - 400 cm^{-1} and are presented in Fig. 3. The absorption bands around 430 cm^{-1} and 580 cm^{-1} are the two featured bands of M-type hexaferrites which were observed in all the samples with minor variations in the position and relative intensities. The band observed around 430 cm^{-1} relates to the octahedral Fe-O bond while the band around 580 cm^{-1} is due to stretching vibrations of the tetrahedral Ba-O bond [31, 32]. The presence of these bonds confirmed the formation of the BaM hexagonal structure. The doublet peak at 2361 cm^{-1} is from ambient CO_2 gas.

3.3 Raman analysis

Raman spectra of the hexaferrite samples are given in Fig. 4. According to group theory, 42 active Raman modes $\Gamma_{Raman} = 11A_{1g} + 14E_{1g} + 17E_{2g}$ arise due to vibrations of 64 atoms at various sites in the unit cell [33]. In our samples, active Raman modes are observed around 284.71, 335.22, 410.28, 457.21, 522.13, 613.52, and 684.87 cm^{-1} which confirms the formation of the BaM phase. The peaks present around 684.87 cm^{-1} are due to the A_{1g} vibration of Fe-O bonds at the octahedral $4f_1$ site and bipyramidal 2b site. Furthermore, the peaks and 457.21 cm^{-1} also due to the A_{1g} vibration of Fe-O bonds at the octahedral 2a. The peaks around 613.52 cm^{-1} and 410.28 cm^{-1} are attributed to the A_{1g} vibration of Fe-O bonds at the octahedral $4f_2$ and 12k sites respectively. The Raman modes observed around 522.13 cm^{-1} and 284.71 cm^{-1} attributed to E_{1g} vibration. Moreover, the peaks at 335.22 cm^{-1} are assigned to the E_{2g} vibrations. The small variations found in the peak positions are attributed to the substitution of Ni^{2+} ions in BaM lattice [31, 34-36].

3.4 UV-vis analysis

The absorption spectra and optical energy bandgap are related as given in Tauc's relation $\alpha\,(h\nu) = A\,(h\nu - E_g)^n$ [37-39], where "A" and "α" represent a constant and absorption coefficient, respectively. While "n" exhibits the values of 1/2 for direct and 2 for indirect transitions. The Tauc's plots of the prepared samples are presented in Fig. 5. The obtained values of optical energy bandgaps lie in the range of 1.21 - 3.39 eV and are plotted as a function of Ni^{2+} ions content as shown in Fig. 6. It can be seen from Fig. 6 that optical bandgap is drastically decreased with the incorporation of a small amount of Ni^{2+} up to x = 0.2, however, a further increase in Ni^{2+} concentration does not have a significant effect on the

bandgap values [26, 31, 40-44]. The results suggest that the synthesized samples are potential candidates for various optoelectronic applications.

3.4 Magnetic Hysteresis loop analysis

The magnetic hysteresis (*M-H*) loops of synthesized nano hexaferrite samples are recorded at 300 K and are depicted in Fig. 7. The *M-H* loops of all the samples show the hard magnetic nature. Different magnetic parameters including saturation magnetization (M_s), magnetic retentivity (Mr), coercivity (H_c), and squareness ratio (M_r/M_s) are measured from *M-H* loops and are given in Table 3. The maximum value of saturation magnetization is observed as 99.92 emu/g for the sample with x = 0 and it reduced to 40.8 emu/g for the sample with x = 0.5. According to previous research, Fe^{3+} ions exhibit various magnetic moments at different sites. As a result, the preferred sites of magnetic Ni^{2+} ions determine the material's overall magnetization. The Ni^{2+} has magnetic nature, but a low magnetic moment as compared to Fe^{3+}. It has been reported earlier that Ni^{2+} ions prefer to substitute Fe^{3+} ions at $4f_2$ and 12k for low concentration and 12k sites for higher concentration. The substitution of Ni^{2+} ($2\mu_B$) ions at the Fe^{3+} ($5\mu_B$) ions sites is responsible for the decrease in saturation magnetization with an increase in Ni^{2+} concentration [15, 20, 31, 45]. The saturation magnetization values which are achieved in this study for Ni^{2+} free samples are compared with the reported values in the literature [4, 9, 20, 45-47] and are found to be significantly higher. The higher values of saturation magnetization achieved are attributed to the vacancy-free samples and occupation of paramagnetic La^{3+} cations at spin up (12k, 2a, and 2b sites) [48, 49]. The magnetic retentivity Mr, coercivity Hc, and squareness ratio (Mr/Ms) also decreased with an increase in Ni^{2+} content and the graphical representation of Ni^{2+} contents *versus* saturation magnetization (M_s) and magnetic retentivity (Mr) as shown in Fig. 8. The magneto-crystalline anisotropy is known to be responsible for the variation in magnetic retentivity, coercivity, and squareness ratio values in ferrite materials [20]. The microwave frequency (ω_m) determined using relation $\omega_m = 8\pi^2 M_s \gamma$, where γ is a gyromagnetic fraction with the significance of 2.8 MHz/Oe, and M_s saturation magnetization [50]. The applied field *versus* microwaves operating frequency (ω_m) of as-prepared hexaferrites samples is plotted in Fig. 9. It can be found from Fig. 9 that the range of microwaves operating frequency (ω_m) is 8.80 – 22.2 GHz, indicating that as-prepared hexaferrites are applicable in longitudinal recording media, data storage magnetic devices, and microwave absorbance purposes.

Conclusions

BaM nano ferrites with the general formula $Ba_{0.8}La_{0.2}Fe_{12-x}Ni_xO_{19}$ ($0 \leq x \leq 0.5$) were synthesized by the co-precipitation route. The prepared powders were densified using conventional sintering processing at 1000 ^{o}C for 4 h. The phase confirmation and structural analysis were carried out using XRD and the average crystallite size of the samples was found in the range 25.2 ± 0.1 – 28.5 ± 0.1 nm. The optical properties of the prepared samples were investigated using UV-vis spectroscopy and it was found that the optical energy bandgap lies in the range 1.21 -3.39 eV. A high value of saturation magnetization *M*s (99.92 emu/g) was achieved for the sample with x = 0, which makes La-BaM hexaferrites suitable for operating in the significantly higher frequency range up to 22.2 GHz. The magnetic parameters (*M*s, *M*r, *H*c, and *M*r/*M*s) of the prepared samples show a decreasing trend with an increase in Ni content. The optical and magnetic properties of Ni^{2+} substituted BaM hexaferrites suggest that these samples are potential candidates for magnetic storage, microwave frequency absorption devices, and magneto-optic devices.

Acknowledgment

The current research is supported by Taif University Researchers Supporting Project number (TURSP-2020/293), Taif University, Taif, Saudi Arabia.

Declaration of Interests

The authors declare that they have no known competing financial interests or personal relationships that could have appeared to influence the work reported in this paper.

References

[1] Jayakumar T, Raja C R and Arumugam S 2020 *Journal of Materials Science: Materials in Electronics* **31** 16308.

[2] Akbarzadeh A, Samiei M and Davaran, S 2012 *Nanoscale research letters* **7** 1

[3] Waqar M, Rafiq M A, Mirza T A, Khalid F A, Khaliq A, Anwar M S and Saleem M 2018 *Applied Physics A* **124** 1

[4] Ramzan M, Arshad M I, Sharif M, Mahmood K, Ali A, Amin N and Ajaz-un-Nabi M 2019 *Journal of Superconductivity and Novel Magnetism* ***32*** 3517

[5] Almessiere M A, Slimani Y, El Sayed H S and Baykal A 2018 *Journal of Sol-Gel Science and Technology* ***88*** 628

[6] Singhal S, Garg A N and Chandra K 2005 *Journal of Magnetism and Magnetic Materials* ***285*** 193

[7] Pullar R C 2012 *Progress in Materials Science* ***57*** 1191

[8] Yasmin N, Yasmin S, Zahid M, Gillani S F, Islam M U, Altaf M and Mirza M 2020 *Physica B: Condensed Matter* ***581*** 411950.
[9] Cernea M, Greculeasa S G, Radu R, Aldica G, Ganea P, Surdu V A and Costescu R M 2020 *Journal of Alloys and Compounds* ***831*** 154850
[10] Mitra C, Ram S and Venimadhav A 2012 *Journal of alloys and compounds* ***545*** 225
[11] Li Y, Wang Q and Yang H 2009 *Current applied physics* ***9*** 1375
[12] Özgür Ü, Alivov Y and Morkoç H 2009 *Journal of Materials Science: Materials in Electronics* ***20*** 789
[13] Janasi S R, Rodrigues D, Landgraf F J and Emura M 2000 *IEEE Transactions on magnetics* ***36*** 3327
[14] Beevers J E, Love C J, Lazarov V K, Cavill S A, Izadkhah H, Vittoria C and Dhesi S S 2018 *Applied Physics Letters* ***112*** 082401.
[15] Baykal A, Auwal I A, Güner S and Sözeri H 2017 *Journal of Magnetism and Magnetic Materials* ***430*** 29
[16] Ramzan M, ARSHAD M, Amin N, Mahmood K, ALIa A, Sharif M and Ajaz-Un-Nabi M 2019 *Digest Journal of Nanomaterials and Biostructures* **14** 849
[17] Ounnunkad S 2006 *Solid State Communications* ***138*** 472
[18] Ashiq M N, Ehsan M F, Iqbal M J and Najam-ul-Haq M 2013 *Journal of Magnetism and Magnetic Materials* ***332*** 93
[19] Iqbal M J and Farooq S 2010 *Journal of Alloys and Compounds* ***505*** 560
[20] Behera P and Ravi S 2019 *Solid State Sciences* ***89*** 139
[21] Güner S, Auwal I A, Baykal A and Sözeri H 2016 *Journal of Magnetism and Magnetic Materials* ***416*** 261
[22] Sözeri H, Küçük İ L K E R and Özkan H 2011 *Journal of Magnetism and Magnetic Materials* ***323*** 1799
[23] Li C J, Wang B and Wang J N 2012 *Journal of Magnetism and Magnetic Materials* ***324*** 1305
[24] Vinnik D A, Zherebtsov D A, Mashkovtseva L S, Nemrava S, Semisalova A S, Galimov D M and Niewa R 2015 *Journal of Alloys and Compounds* ***628*** 480
[25] Tang X, Yang Y and Hu K 2009 *Journal of Alloys and Compounds* ***477*** 488
[26] Ashraf G A, Zhang L, Abbas W and Murtaza G 2019 *Current Applied Physics* ***19*** 506
[27] Jamalian M, Ghasemi A and Asl M J P 2015 *Journal of Electronic Materials* ***44*** 2856
[28] Cullity B D 1978 *Plane Spacings" in lattice geometry In Elements of X-Ray Diffraction* Addison-Wesley publishing company Inc. MI USA

[29] El-Sayed S M, Meaz T M, Amer M A and El Shersaby H A 2014 *Particulate Science and Technology* ***32*** 39

[30] Amjad T, Sadiq I, Javaid A B, Riaz S, Naseem S and Nadeem M 2019 *Journal of Alloys and Compounds* ***770*** 1112

[31] Auwal I A, Baykal A, Güner S, Sertkol M and Sözeri H *Journal of Magnetism and Magnetic Materials* ***409*** 92

[32] Kaur T, Kumar S, Bhat B H, Want B and Srivastava A K 2015 *Applied Physics A* ***119*** 1531

[33] Kreisel J, Lucazeau G and Vincent H 1998 *Journal of Solid-State Chemistry* ***137*** 127

[34] Wu C, Yu Z, Yang Y, Sun K, Nie J, Liu Y and Lan Z 2016 *Journal of Alloys and Compounds* ***664*** 406

[35] Buzinaro M A P, Ferreira N S, Cunha F and Macêdo M A 2016 *Ceramics International* ***42*** 5865

[36] Morel A, Le Breton J M, Kreisel J, Wiesinger G, Kools F and Tenaud P 2002 *Journal of magnetism and magnetic materials* ***242*** 1405

[37] Ashraf G A, Zhang L, Abbas W and Murtaza G 2018 *Ceramics International* ***44*** 18678

[38] Aslam A, Razzaq A, Naz S, Amin N, Arshad M I, Nabi M A U and Ur Rehman A 2021 *Journal of Superconductivity and Novel Magnetism* 1

[39] Aslam A, Rehman A U, Amin N, un Nabi M A, ul ain Abdullah Q, Morley N A and Mehmood K 2021 *Journal of Physics and Chemistry of Solids* ***154*** 110080

[40] Karmakar M, Mondal B, Pal M and Mukherjee K 2014 *Sensors and Actuators B: Chemical* ***190*** 627

[41] Valero-Luna C, Palomares-Sanchéz S A and Ruíz F 2016 *Catalysis Today* ***266*** 110

[42] Hussain K, Amin N and Arshad M I 2021 *Ceramics International* ***47*** 3401

[43] ALIa I, Amin N, Rehman A, Akhtar M, Fatima M, Mahmood K and Arshad M I 2020 *Digest Journal of Nanomaterials & Biostructures* ***15*** 1

[44] Amin N, Akhtar M, Sabir M, Mahmood K, ALIa A, Mustafa G and Arshad M 2020 *Journal of Ovonic Research* ***16*** 11

[45] Alsmadi A M, Bsoul I, Mahmood S H, Alnawashi G, Prokeš K, Siemensmeyer K and Nakotte H 2013 *Journal of Applied Physics* ***114*** 243910

[46] Kamzin A S, Rozenbaum V L and Ol'khovik L P 1999 *Physics of the Solid State* ***41*** 433

[47] Afghahi S S S, Jafarian M, Salehi M and Atassi Y 2017 *Journal of Magnetism and Magnetic Materials* ***421*** 340

[48] Liu X, Zhong W, Yang S, Yu Z, Gu B and Du Y 2002 *Journal of Magnetism and Magnetic Materials* ***238*** 207

[49] Liu X, Hernandez-Gomez P, Huang K, Zhou S, Wang Y, Cai X and Ma B 2006 *Journal of magnetism and magnetic materials* ***305*** 524

[50] Rehman A U, Morley N A, Amin N, Arshad M I, un–Nabi M A, Mahmood K and Alzaid M 2020 *Ceramics International* ***46*** 29297

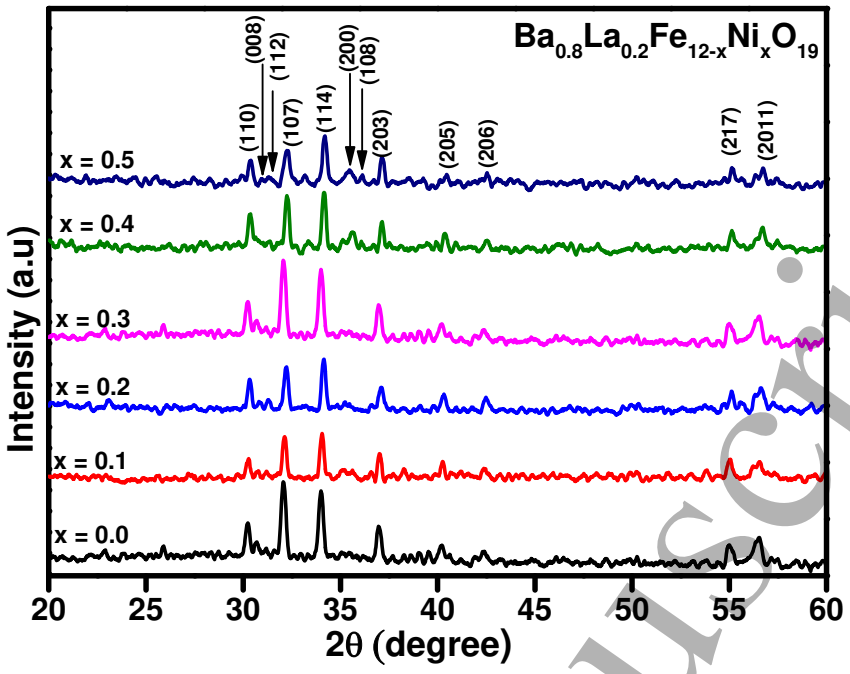

Fig. 1 XRD patterns of synthesized $Ba_{0.8}La_{0.2}Fe_{12-x}Ni_xO_{19}$ hexaferrite powders.

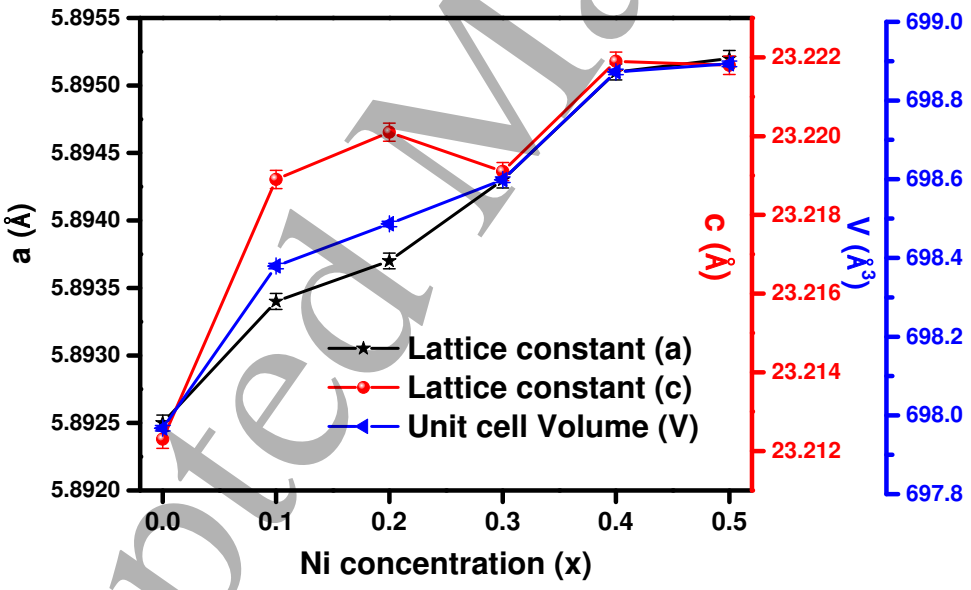

Fig. 2 Plot of Lattice parameters (*a* & *c*) and unit cell volume (*V*) as a function of Ni^{2+} content in the synthesized hexaferrite samples.

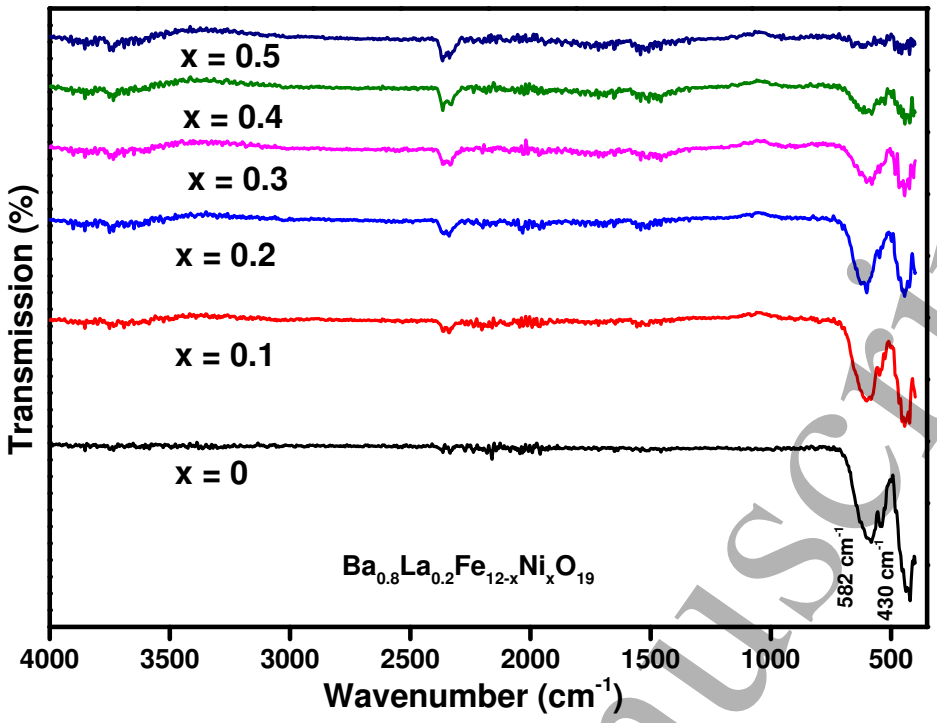

Fig. 3 FTIR spectra of as-synthesized hexaferrite samples.

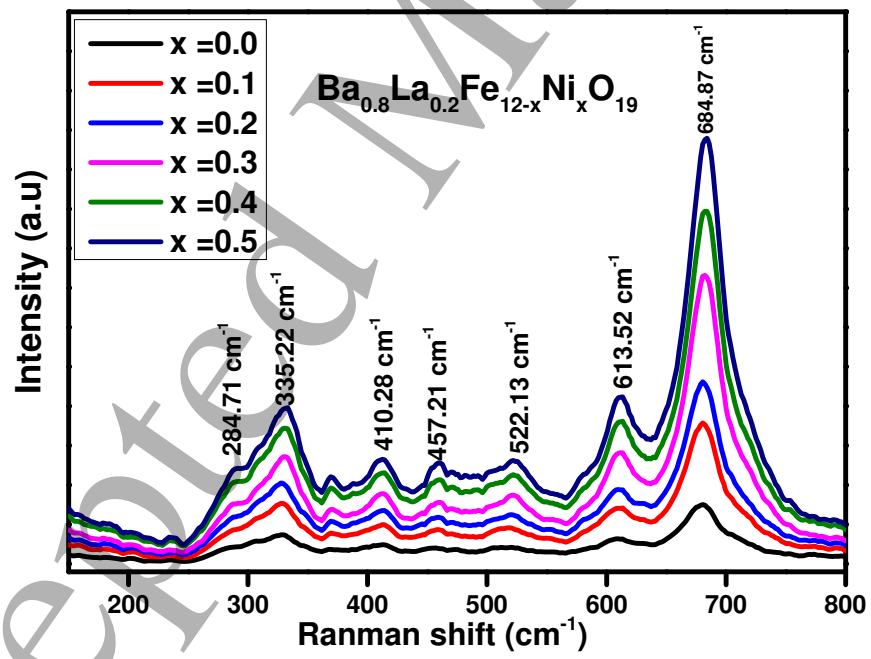

Fig. 4 Raman spectra of Ni^{2+} substituted Ba-La hexaferrite samples.

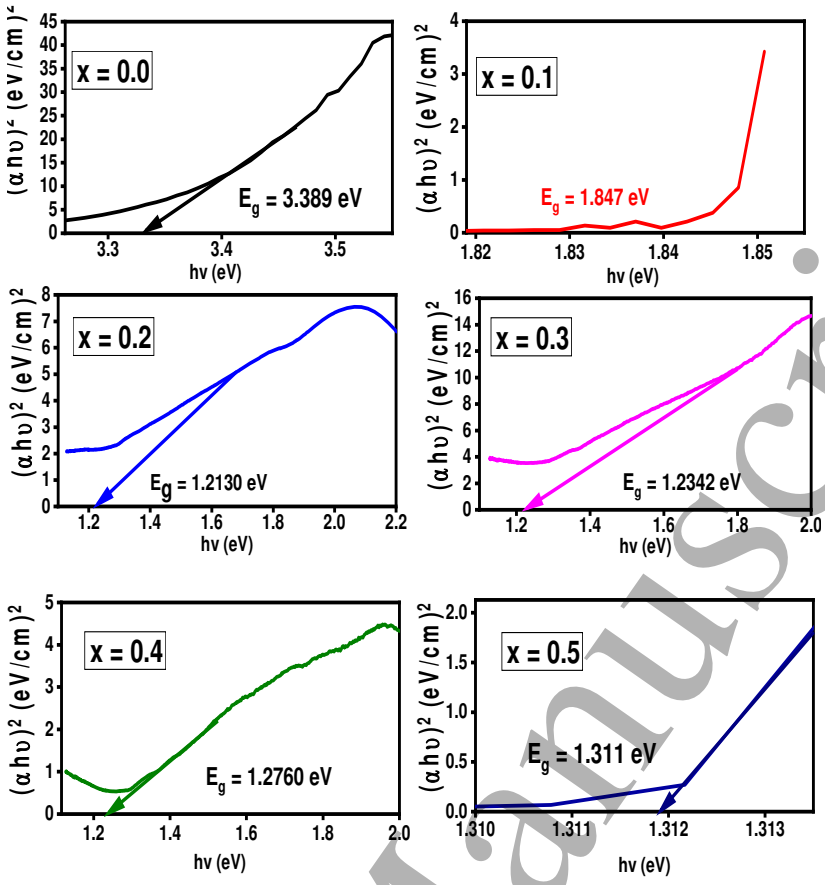

Fig. 5 Plot of $(\alpha h\upsilon)^2$ *versus* photon energy ($h\upsilon$) for prepared hexaferrite nanoparticles.

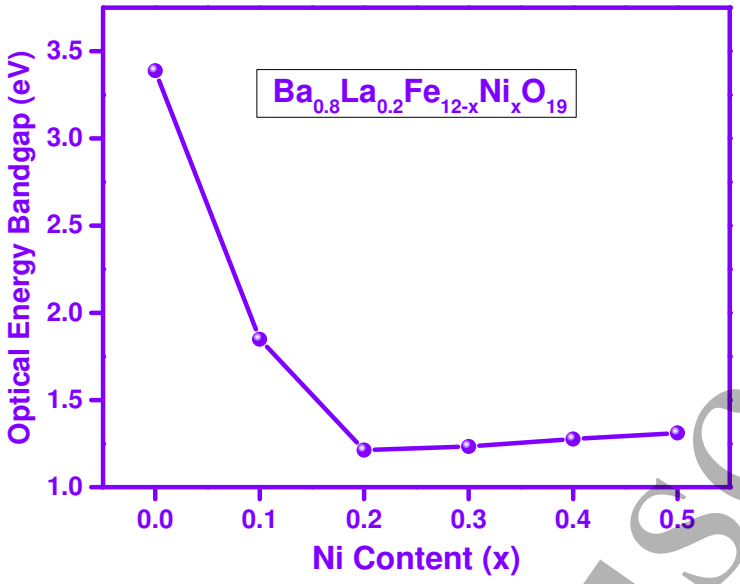

Fig. 6 Plot of energy bandgap as a function of Ni^{2+} ions content

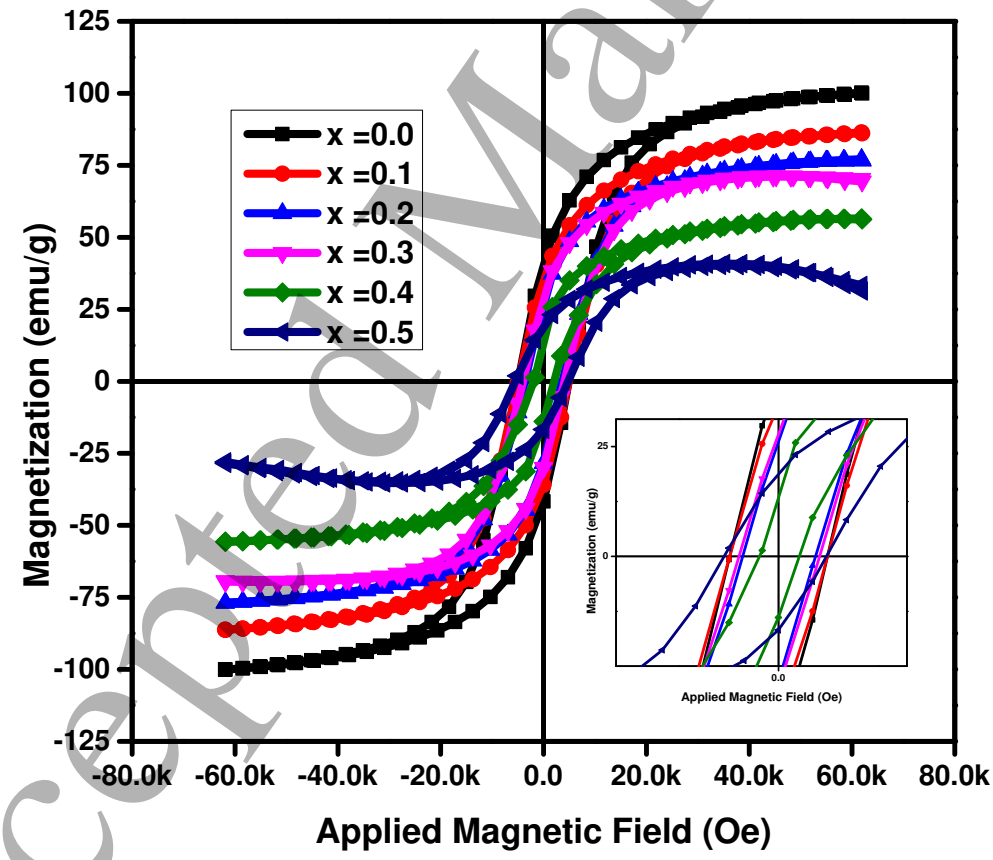

Fig. 7 *M-H* loops for Ni^{2+} doped Ba-La hexaferrites.

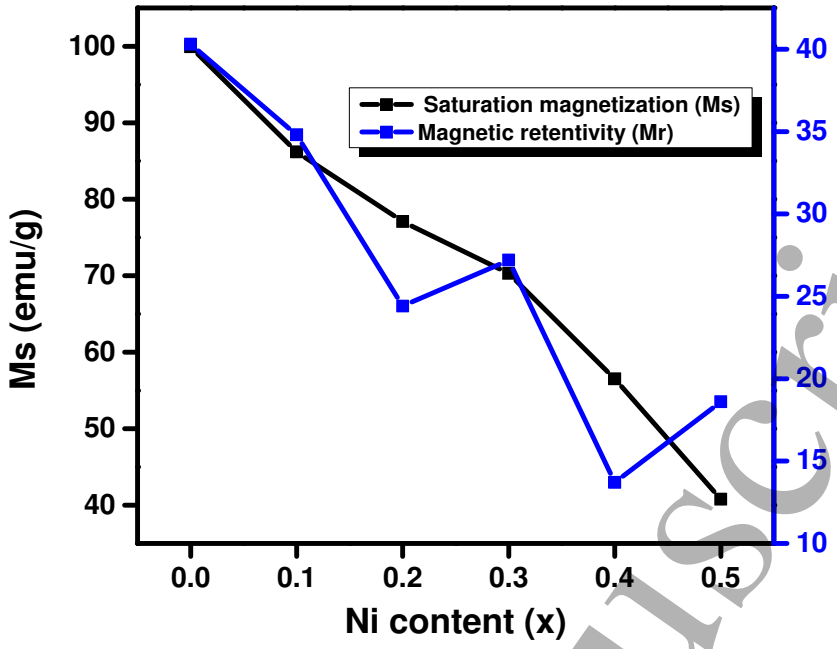

Fig. 8 Plot of saturation magnetization and remanent magnetization of synthesized samples as a function of Ni content

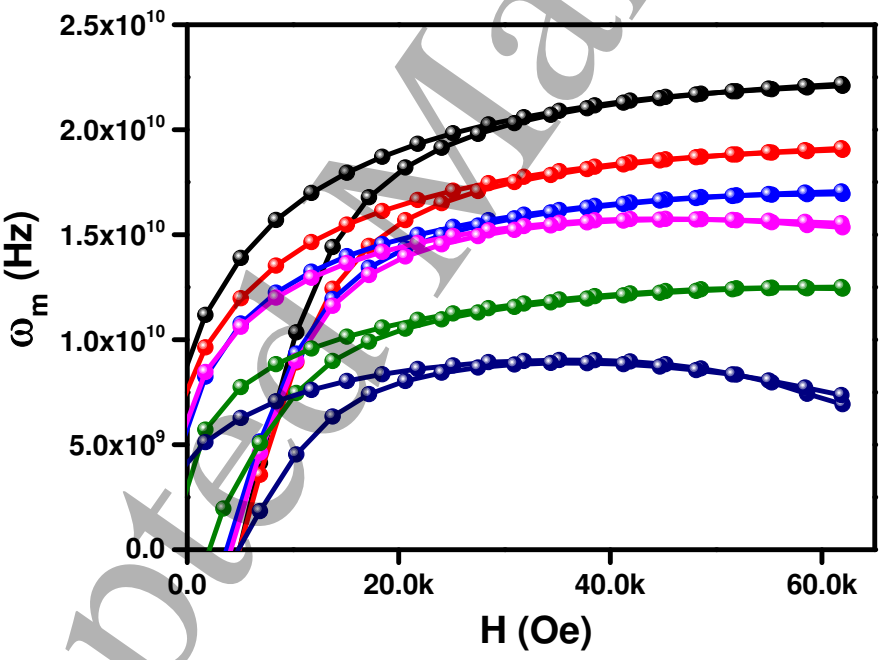

Fig. 9 Applied field *versus* microwaves operating frequency

Table 1. Concentrations of Ni^{2+} and calculated structural parameters of $Ba_{0.8}La_{0.2}Fe_{12-x}Ni_xO_{19}$ hexaferrites.

Parameters	***x* = 0.0**	***x* = 0.1**	***x* = 0.2**	***x* = 0.3**	***x* = 0.4**	***x* = 0.5**
Lattice parameter *a* (Å) ± 0.001	5.8925	5.8934	5.8937	5.8943	5.8951	5.8952
Lattice parameter *c* (Å) ± 0.001	23.2123	23.2189	23.2201	23.2191	23.2219	23.2218
Unit cell Volume *V* ($Å^3$) ± 0.006	697.96	698.37	698.48	698.59	698.87	698.89
Crystallite size *D* (nm) ±0.1	27.9	28.5	27.8	26.6	26.2	25.2
X-ray density D_X (g/cm^3)	5.310	5.299	5.304	5.144	5.229	5.219
Dislocation Density ρ (10^{11} cm^{-2})	1.280	1.227	1.291	1.413	1.460	1.579

Table 2. Elemental Composition of $Ba_{0.8}La_{0.2}Fe_{12-x}Ni_xO_{19}$ M-type hexaferrites obtained from EDX

Samples	**Elemental composition (%)**				
	Ba	**La**	**Ni**	**Fe**	**O**
$Ba_{0.8}La_{0.2}Fe_{12}O_{19}$	2.52	0.64	0.00	37.29	59.55
$Ba_{0.8}La_{0.2}Fe_{11.9}Ni_{0.1}O_{19}$	2.51	0.65	0.31	36.92	59.61
$Ba_{0.8}La_{0.2}Fe_{11.8}Ni_{0.2}O_{19}$	2.60	0.61	0.63	37.16	59.00
$Ba_{0.8}La_{0.2}Fe_{11.7}Ni_{0.3}O_{19}$	2.56	0.63	0.94	36.22	59.65
$Ba_{0.8}La_{0.2}Fe_{11.6}Ni_{0.4}O_{19}$	2.49	0.64	1.27	35.72	59.88
$Ba_{0.8}La_{0.2}Fe_{11.5}Ni_{0.5}O_{19}$	2.69	0.64	1.54	35.69	59.44

Table 3. Magnetic parameters of as-prepared hexaferrites

Samples	***M*s** (emu/g)	***M*r** (emu/g)	***H*c** (Oe)	***M*r/*M*s**	ω_m **(GHz)**
$Ba_{0.8}La_{0.2}Fe_{12}O_{19}$	99.92	40.3	5132.9	0.40332	22.2
$Ba_{0.8}La_{0.2}Fe_{11.9}Ni_{0.1}O_{19}$	86.2	34.8	5037.7	0.40371	19.2
$Ba_{0.8}La_{0.2}Fe_{11.8}Ni_{0.2}O_{19}$	77.1	24.4	3336.3	0.31647	17.1
$Ba_{0.8}La_{0.2}Fe_{11.7}Ni_{0.3}O_{19}$	70.3	27.2	3217.2	0.38691	15.7
$Ba_{0.8}La_{0.2}Fe_{11.6}Ni_{0.4}O_{19}$	56.5	13.7	1154.9	0.24248	12.6
$Ba_{0.8}La_{0.2}Fe_{11.5}Ni_{0.5}O_{19}$	40.8	18.6	2034.8	0.45588	8.80